Analysis of EMI from Pantograph-catenary Arc on Speed Sensor Based on the High-speed Train Model

Yutao Tang, Feng Zhu, and Yingying Chen

School of Electrical Engineering
Southwest Jiaotong University, Chengdu, 610031, China
tangyutao@my.swjtu.edu.cn, zhufeng@swjtu.edu.cn, 454621625@qq.com

Abstract ─ There will be the pantograph-catenary arc (PCA) when the pantograph of a high-speed train is separated from the power supply line, and the electromagnetic interference (EMI) caused by the PCA can affect speed sensors of the train. To study the influence of the PCA, firstly, the traction control unit (TCU) speed sensor of the high-speed train is researched. The result shows both overvoltage and electromagnetic radiation (EMR) generated by the PCA can influence the signal of speed sensor. Secondly, the composite model of the train is established. Then, the interference of the PCA on the TCU speed sensor is verified. The results of practical measurements show the PCA causes a maximum overvoltage of 680 V on train body (TB) and increases the magnetic field around TB to a maximum of 58 dBμA/m. This is the reason of sensor malfunction, which is consistent with the theoretical and simulation results. Finally, the methods to reduce the EMI of the PCA are proposed.

Index Terms ─ Electromagnetic Interference (EMI), high-speed train, overvoltage, Pantograph-Catenary Arc (PCA), speed sensor.

I. INTRODUCTION

The high-speed train gets electric energy from the power supply line by the pantograph. But the pantograph needs to be separated from the line after the train stops stably. The pantograph-catenary arc (PCA) will be produced at the moment when the pantograph is separated from the line [1]-[3], and the electromagnetic interference (EMI) of the PCA affects the electronic equipment on the train, such as speed sensor. A typical example is the train doors cannot be opened normally after the train stops at a station in China. According to the analysis results of the door control unit (DCU), there are two ways to close the train doors. Firstly, the driver can send the door closing command to DCU directly to close all the doors. Secondly, the traction control unit (TCU) speed sensors transmit the detected speed to TCU. As long as the speed detected by one of the TCU speed sensors exceeds 5 km/h, all the train doors will be closed automatically [4, 5]. After the train arrives at the station and stops stably, the driver will not issue the directive to close the doors, and the train speed shall be zero. But the fact is the train doors still cannot be opened normally. Therefore, the PCA is likely to interfere with the speed sensor and cause it to malfunction. So, it is necessary to research the EMI caused by the PCA.

Some scholars have used the train model to study the overvoltage on the train bodies (TBs) when the pantograph is separated from the power supply line [6]-[8]. But they did not study the effect of overvoltage on the speed sensors. The electromagnetic radiation (EMR) caused by the PCA of the subway has been measured and analyzed in [9, 10]. But its characteristics are different from those of high-speed trains. In some studies [11, 12], researchers analyzed the working principle of speed sensors and researched the effect of the PCA on it. But they only considered a single influence factor and did not combine the complete train model to study the influence of multiple disturbances.

As an extension of previous works, firstly, the structure and interference modes of the TCU speed sensor on a high-speed train are analyzed. The results show that the sensor signal is impacted by overvoltage and EMR generated by the PCA. Secondly, the structure of the Chinese high-speed train is studied in detail and the composite model is established. The model includes the power supply line, TBs, speed sensors, grounding systems, and PCA. Thirdly, the practical measurements are carried out when the pantograph on the roof of the second TB (02TB) is separated from the power supply line. The results show the maximum value of overvoltage on the 02TB is approximately 680 V, and the magnetic field around the 02TB is nearly 58 dBμA/m. Therefore, the signal of the TCU speed sensor can be affected by the PCA. Finally, the methods of adding protective earthing and nesting magnetic rings are proposed to reduce the EMI caused by the PCA on the TCU speed sensor.

Submitted On: October 4, 2020
Accepted On: December 3, 2020

https://doi.org/10.47037/2020.ACES.J.360213

II. ANALYSIS OF THE STRUCTURE AND INTERFERENCE MODES OF TCU SPEED SENSOR

A. Structure of the high-speed train with TCU speed sensors

The Chinese high-speed train consists of 16 TBs. Besides, there are a pantograph, working earthing, and TCU speed sensor on the 02TB, 07TB, 10TB, and 15TB, respectively [13]. There is one protective earthing between the 08TB and 09TB. The partial structure of the high-speed train is shown in Fig. 1.

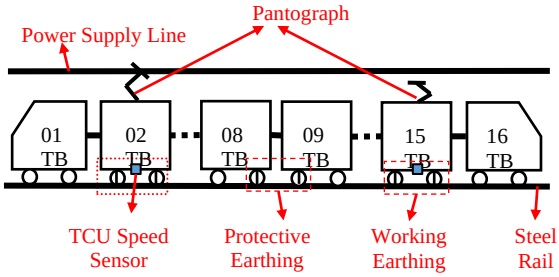

Fig. 1. The partial structure of the high-speed train.

B. Interference of the PCA on TCU speed sensors

The PCA is generated at the moment when the pantograph is separated from the power supply line, which produces EMR and overvoltage on the TBs.

Only one end of the TCU speed sensor cable is connected to the TB as shown in Fig. 2 (a). The overvoltage caused by the PCA creates a parasitic capacitance between the cable shield and the core wire of the sensor as shown in Fig. 2 (b).

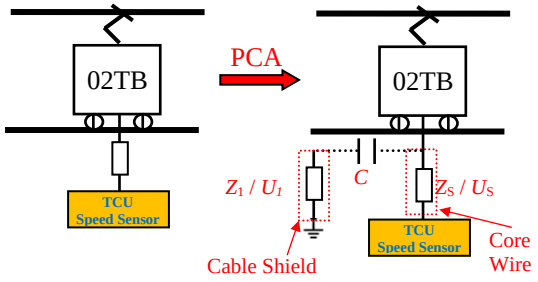

Fig. 2. Connection diagram of TCU speed sensor before and after the pantograph separation.

According to Fig. 2 (b), the inductive voltage generated by the overvoltage on the sensor core wire can be calculated by:

$$U_s = \frac{jwCZ_s}{1+ jwC(Z_1 + Z_s)} U_1, \quad (1)$$

where U_s is the interference voltage, which can impact the signal of the TCU speed sensor. Z_1 and Z_s are the impedance of sensor cable shield and core wire, respectively, U_1 is the overvoltage between the sensor cable shield and the steel rail, and C is the parasitic capacitance generated by the overvoltage [12].

In addition, the EMR from the PCA can also affect the TCU speed sensors. The outer conductor of the sensor cable is made of metal wires. Because there are many small holes, the outer conductor is not completely shielded. The inductive electric field (E) is generated on the surface of the cable because of the EMR. As described in Fig. 3, a part of the inductive electric field (E') will be coupled on the core wire by the tiny holes. Because the $E > E$', the potential difference (U) between the cable shield and core wire can be caused.

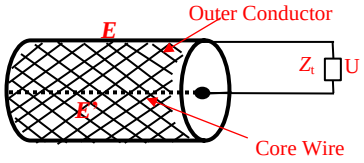

Fig. 3. The diagram of speed sensor cable.

The value of U can be obtained by [14]:

$$U = I \times Z_t \times L_m, \quad (2)$$

where I is the inductive current, Z_t is the transfer impedance per meter cable, and L_m is the effective length of the cable.

Based on the above analysis, the overvoltage and the EMR are two different interference modes of the PCA to TCU speed sensor. They cause the inductive voltage on the core wire and the potential difference between the cable shield and core wire respectively. Besides, they can affect the signal port of the sensor and make it detect the wrong speed signal, which lead to the malfunction of the DCU.

III. COMPOSITE MODEL OF THE HIGH-SPEED TRAIN

A. Structure of the high-speed train model

When the high-speed train is running, the pantograph is connected to the power supply line (25 kV / 50 Hz). The current is transmitted to four traction transformers at 02TB, 07TB, 10TB, and 15TB. In addition, four TCU speed sensors are respectively installed on the wheel shaft end of that TBs.

As shown in Fig. 4, the current flows into the earth by working earthings on the primary side of the transformer. Besides, the high voltage cable, sixteen TBs, and steel rail are also included in the composite model. There is a switch to simulate the separation of the pantograph and the power supply line by opening it. The relevant parameters in the model refer to the equivalent parameters of the Beijing-Tianjin high-speed railway in China as listed in Table 1 [15].

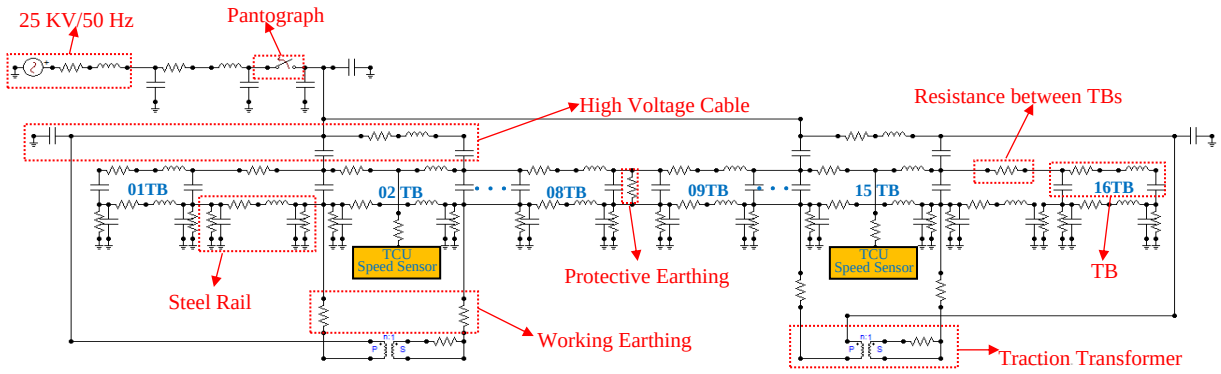

Fig. 4. The diagram of the composite model of the high-speed train.

Table 1: Relevant parameters of the train model

Name	Parameter Name	Parameter Value
TB	Resistance	0.225 mΩ
	Inductance	0.001103375 mH/m
	Capacitance	0.00001007011316 μF/m
	Resistance Between TBs	6.4mΩ
	Length	25 m/TB
Steel Rail	Resistance	0.1367 mΩ/m
	Inductance	0.000429718 mH/m
	Capacitance	0.0000603384 μF/m
	Leakage conductance	0.01 mS/m
Transformer	Equivalent Resistance	2.941 Ω
Protective Earthing	Resistance	0.05 Ω
Working Earthing	Resistance	0.05 Ω

Besides, an arc model will be added to the model to simulate the PCA when the pantograph is separated from the power supply line as described in Fig. 5. The relevant parameters are shown in Table 2.

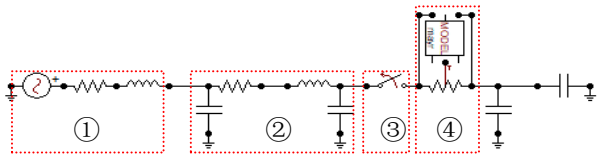

Fig. 5. Model of the PCA generation.

B. Establishment of the PCA model

The current common arc models are Mayr Model, Cassie Model, and Habedank Model [16]. The Habedank Model combines the other two models and makes up for their shortcomings. The mathematical model of Habedank Model is [17]:

$$\begin{cases} \dfrac{dg_C}{dt} = \dfrac{1}{\theta_C}\left(\dfrac{i^2}{u_C \cdot g_C} - g_C\right) \\ \dfrac{dg_M}{dt} = \dfrac{1}{\theta_M}\left(\dfrac{i^2}{P_0} - g_M\right) \\ \dfrac{1}{g} = \dfrac{1}{g_C} - \dfrac{1}{g_M} \end{cases}, \tag{3}$$

where g_C, θ_C, g_M, and θ_M are the conductance and the time constants of Mayr and Cassie Model, respectively. u_C, i, and P_0 are the voltage, current, and dissipative power of arc. P_0 is assumed to be constants in Eq. (3). In fact, it is not constant and needs to be modified to create a more realistic PCA model.

Table 2: Relevant parameters of the model of the PCA generation

No.	Name	Parameter Name	Parameter Value
①	Railway Traction Substations	Voltage	25 KV / 50 Hz
		Resistance	0.165 Ω
		Inductance	10.8 mH
②	High Voltage Cable	Resistance	0.014 mΩ/m
		Inductance	0.000131093 mH/m
		Capacitance	0.00041162 μF/m
③	Pantograph	--	--
④	PCA Model	--	--

The diameter (d) and the convective power (P_k) of the PCA will be changed because of the train speed [18]. P_k of the PCA can be calculated by [19]:

$$P_k' = 0.1464 d (v + 36)^{1.5}, \tag{4}$$

where P_k' is P_k per unit length of the PCA. v is the train speed, which unit is km/h .

The d value is changed by the transverse airflow [20]. The relationship between d and v is:

$$d = 1.5369\sqrt{\frac{i}{v+36}}. \tag{5}$$

P_k' can be derived by Eq. (4) and Eq. (5):

$$P_k' = 0.225\sqrt{i}(v+36). \tag{6}$$

After the train stops, the PCA will be generated at the moment the pantograph is separated from the power supply line. At this moment, the maximum length of the PCA (L_{arc}) is 10 mm and v is 0 km/h. P_k can be obtained by:

$$P_k = 81\sqrt{i}. \tag{7}$$

P_k and the radiation power (P_s) of the PCA account for approximately 80% and 20% of P_0, respectively. So P_0 of the PCA is:

$$P_0 = 101.25\sqrt{i}. \tag{8}$$

According to [21], u_C of the PCA is only related to the length of the arc, and the proportion is a positive constant. u_C of the PCA is calculated by:

$$u_C = 15L_{arc}, \tag{9}$$

where factor 15 is an empirical value when the voltage of the power supply line is 25 KV/50 Hz.

The new PCA model can be derived by Eq. (3) ~ Eq. (9):

$$\begin{cases} \dfrac{dg_C}{dt} = \dfrac{1}{\theta_C}\left(\dfrac{i^2}{150g_C} - g_C\right) \\ \dfrac{dg_M}{dt} = \dfrac{1}{\theta_M}\left(\dfrac{i^{1.5}}{101.25} - g_M\right) \\ \dfrac{1}{g} = \dfrac{1}{g_C} - \dfrac{1}{g_M} \end{cases}. \tag{10}$$

C. Simulation results of the high-speed train model

The simulation results show that the distribution of TB voltage is uniform when the high-speed train is running (the switch is closed). As we can see in Fig. 6, the maximum difference of TB voltage (from the head to the tail of the train, total length is 400 m) is only 0.0036 V, which can be neglected. However, the pantograph will be separated from the power supply line after the train stops (the switch is opened). At this moment, the PCA produces large overvoltage on TB where the pantograph is located. But overvoltage can be discharged by protective grounding. Therefore, the overvoltage on the TBs far away from the pantograph and close to the protective grounding is small (such as 08TB and 09TB). So the distribution of TB voltage is extremely uneven when the pantograph is separated from the line. The maximum TB voltage is nearly 700 V (on the 02TB). But the TB voltage on the 08TB and 09TB is much lower than that on the other TBs, which is only around 50 V as shown in Fig. 7.

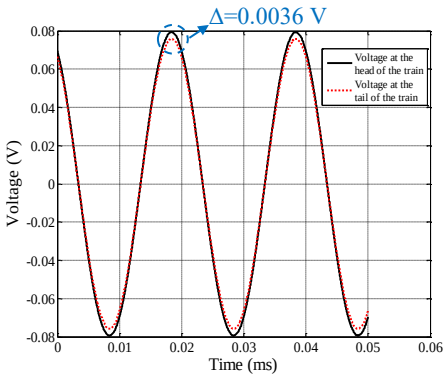

Fig. 6. The TB voltage at the head and tail of the train.

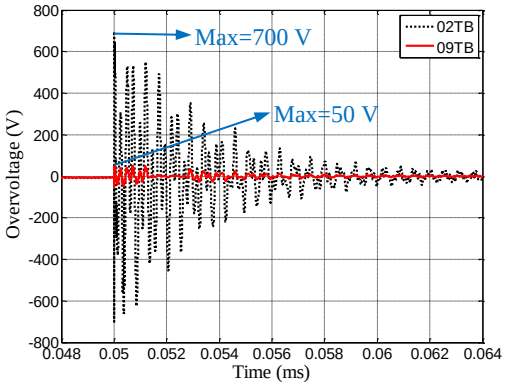

Fig. 7. The overvoltage on 02TB and 09TB.

The train and PCA models are based on the Chinese typical high-speed train and the Beijing-Tianjin high-speed railway in this paper. The potential limitations and several differences need to be noted to extend these models to other cases.

1) There are some differences in structure and related parameters among different types of trains. For example, the trains of Japan and Germany have eight train bodies, while there are only four in Brazil. Moreover, the impedance and position of the grounding system are also different. When the model is applied to other types of trains, the impedance, position, and length of the train bodies and the grounding system should be reset.

2) The characteristics of PCA will be affected by the running environment of trains. The unstable route will aggravate the PCA generation, and the moist or dry air will change the radiation characteristics of the PCA. Therefore, it is necessary to consider the environmental factors in PCA modeling.

3) The model can be used to analyze the EMI on other electrical equipment, like digital encoders, LED display, and temperature sensors. The connection position and electrical structure of the equipment should be

changed accordingly in the model.

IV. MEASUREMENT AND SUPPRESSION OF INTERFERENCE

A. Scenario and results of the measurement

The practical measurements are carried out at a high-speed train station in China. The test items include the TB voltage, magnetic field around the TB, and signal port voltage of the sensor. The pantograph on the 02TB is separated from the power supply line to produce the PCA during the measurement. The relative specifications are listed in Table 3.

Table 3: The specifications of measurement instruments

Instruments		Specifications	
Name	**Model**	**Name**	**Data**
EMI receiver	ESCI-3	Frequency range	9 KHz ~ 3 GHz
		Resolution ratio	0.1 Hz
		Specification	+30 ~ -147 dBm
Loop antenna	HFH2-Z2	Frequency range	9 KHz ~ 30 MHz
Digital multimeter	VC890C	Direct voltage	200 mV ~1000 V
		Alternating voltage	2 ~750 V
Oscilloscope	GDS-2302A	Frequency	500 MHz
		Maximum sampling rate	5 Gsample/s

The 02TB voltage is measured by a digital multimeter as shown in Fig. 8. The results show that the maximum overvoltage on the 02TB is 680 V when the pantograph is separated from the power supply line. It is consistent with the previous simulation results (in Fig. 7).

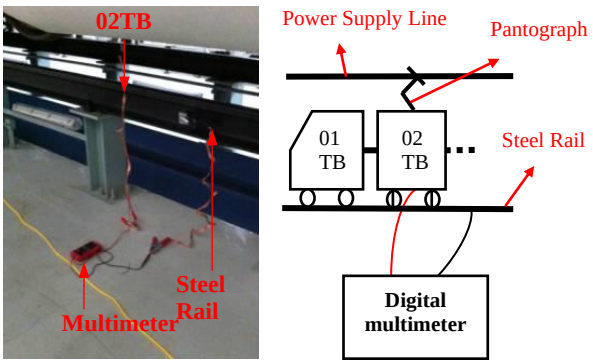

(a) (b)

Fig. 8. Measurement scenario of TB voltage test.

The measurement scenario and results of the magnetic field around the 02TB are shown in Fig. 9 and Fig. 10, respectively. The results show that the magnetic field will increase (up to roughly 58 dBμA/m) because of the PCA.

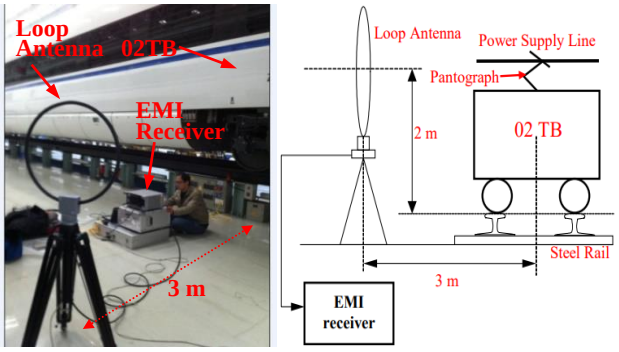

(a) (b)

Fig. 9. Measurement scenario of magnetic field test.

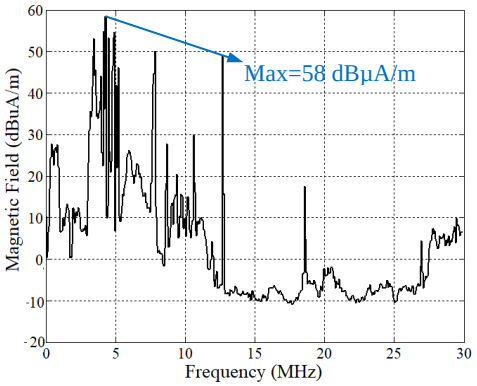

Fig. 10. Measurement results of the magnetic field around the 02TB.

The measurement results show that when the pantograph is separated from the power supply line, the EMI caused by PCA is shown in the following two aspects: Firstly, the interference value of 680 V overvoltage is formed on the TB. Secondly, the magnetic field around the TB is increased, and the strong magnetic field interference is mainly concentrated in 5 MHz and up to 58 dBμA/m. According to the Section II, those two interference modes cause the wrong voltage signal on the TCU speed sensor. The signal port voltage of the sensor is tested by an oscilloscope. In fact, there should not be voltage on the sensor signal port after the train stops. But due to the EMI of PCA, the signal port voltage is approximately 2.6 V when the pantograph is separated as described in Fig. 11. The sensor will be activated if the signal port voltage of speed sensor exceeds 1.5 V. So the EMI of PCA will affect the control of train doors by interfering with TCU speed sensor.

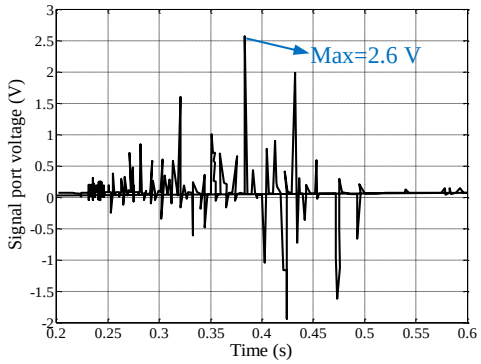

Fig. 11. Signal port voltage of the TCU speed sensor on 02TB.

B. Methods of interference suppression

According to the above research, both the overvoltage and the EMR generated by the PCA can influence the TCU speed sensor.

Firstly, as for the effect from the overvoltage, the interference voltage (U_s) can be restrained by reducing the overvoltage (U_1) as shown in Eq. (1). According to the simulation results in section III, U_1 is greatly reduced by protective earthing. Because the protective earthing is connected to the TBs and the earth, the TB voltage can be discharged by it. But the train has only one protective grounding, which is installed between the 08TB and 09TB (the middle position of the train). A high-speed train is about 400 m, so the overvoltage on the TBs far away from the protective grounding will be very large. Therefore, the new protective earthing can be added on the TBs with higher overvoltage to decrease U_s. Compared with Fig. 11, the signal port voltage of the TCU speed sensor is significantly reduced after the protective earthing is added on the 02TB as shown in Fig. 12.

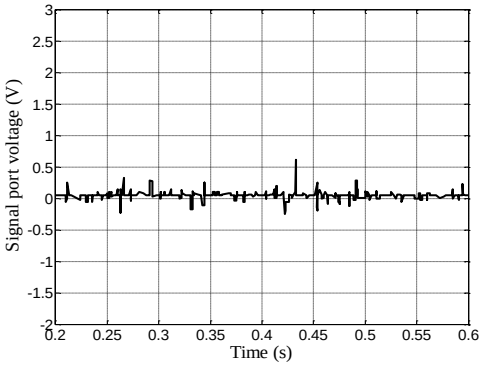

Fig. 12. Signal port voltage of the TCU speed sensor on 02TB after adding a protective earthing.

Secondly, the potential difference (U) between the cable shield and core wire can be reduced to suppress the EMR from the PCA based on Eq. (2). The magnetic rings can absorb the EMR energy and reduce Z_t of cable. Nesting the suitable Ni-Zn ferrite magnetic rings on the cable of the speed sensor can reduce the EMI on the cable. As shown in Fig. 13, the peak of EMI is decreased by about 7 dB after using the magnetic rings. Moreover, the discrete interference is reduced obviously in 10 MHz ~ 30 MHz. The measurement method of the EMI on the speed sensor and the specific selection process of magnetic rings are introduced in detail in another paper of the authors [13].

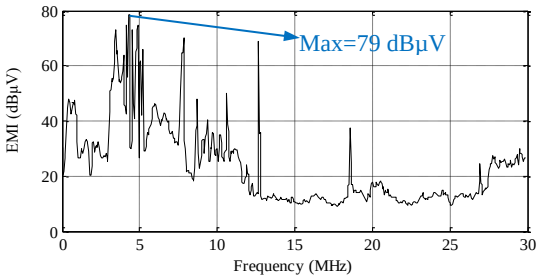

(a) Before nesting the Ni-Zn ferrite magnetic rings

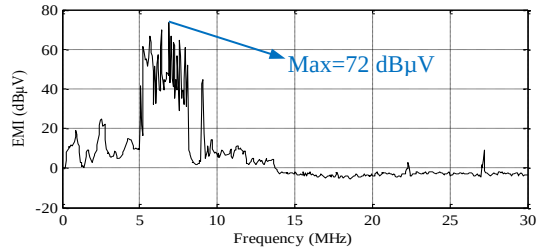

(b) After nesting the Ni-Zn ferrite magnetic rings

Fig. 13. The waveform of EMI on the TCU speed sensor cable.

V. CONCLUSION

The interference of the PCA on the TCU speed sensor of the high-speed train has been measured and analyzed. The conclusions are as follows:

1) The PCA creates the overvoltage (maximum is 680 V) on the TB. Besides, the EMR from the PCA increases the magnetic field to 58 dBμA/m around the TB.

2) The overvoltage can impact the TCU speed sensor signal by the parasitic capacitance between the cable shield and core wire. Also, the EMR can affect the speed sensor by the holes on the sensor cable shield.

3) The overvoltage and EMR caused by the PCA can be effectively suppressed by adding the protective earthing on the train and nesting the Ni-Zn ferrite magnetic rings on the sensor cable respectively.

ACKNOWLEDGMENT

We would like to thank the anonymous reviewers for their insightful comments. This paper is supported

by the National Key R&D Program of China (No. 2018YFC0809500).

REFERENCES

[1] X. Li, F. Zhu, H. Lu, R. Qiu, and Y. Tang, "Longitudinal propagation characteristic of pantograph arcing electromagnetic emission with high-speed train passing the articulated neutral section," *IEEE Transactions on Electromagnetic Compatibility*, vol. 61, no. 2, pp. 319-326, June 2018.

[2] F. Zhu, C. Gao, and Y. Tang, "Influence of pantograph-catenary arc on electromagnetic disturbance of airport terminal omnidirectional beacon," *China Railway Science*, vol. 39, no. 1, pp. 116-121, Jan. 2018.

[3] J. Gou, F. Zhu, J. Zou, J. Ye, H. Li, and Y. Wang, "Research on EMI of instrument landing system on aircraft caused by pantograph arc," *Journal of the China Railway Society*, vol. 40, no. 7, pp. 61-66, July 2018.

[4] K. Huang, Z. G. Liu, F. Zhu, Z. S. Zheng, and Y. Cheng, "Evaluation scheme for EMI of train body voltage fluctuation on the BCU speed sensor measurement," *IEEE Transactions on Instrumentation and Measurement*, vol. 66, no. 5, pp. 1046-1057, May 2017.

[5] F. Zhu, Y. Tang, and C. Gao, "Mechanism and suppression of electromagnetic interference of pantograph-catenary arc to speed sensor of CRH380BL electric multiple unit," *China Railway Science*, vol. 37, no. 6, pp. 69-74, Nov. 2016.

[6] Y. Cheng, Z. Liu, and H. Ke, "Transient analysis of electric arc burning at insulated rail joints in high-speed railway stations based on state-space modeling," *IEEE Transactions on Transportation Electrification*, vol. 3, no. 3, pp. 750-761, Sep. 2017.

[7] Y. Cheng, Z. Liu, H. Ke, and H. Zhou, "Modeling analysis of electric multiple units passing insulated rail joints in high-speed railway station," *IEEE ITEC 2017 Asia-Pacific*, 2017.

[8] F. Fan, "Study on separation between the pantograph and catenary based on improved Habedank arc model," *M.S. Thesis*, Dept. Electr. Eng., Southwest Jiaotong University, Chengdu, China, 2014.

[9] X. Li, F. Zhu, H. Lu, R. Qiu, and Y. Tang, "Longitudinal propagation characteristic of pantograph arcing electromagnetic emission with high-speed train passing the articulated neutral section," *IEEE Trans. IEEE Transactions on Electromagnetic Compatibility*, vol. 61, no. 2, pp. 319-326, June 2018.

[10] X. Li, F. Zhu, R. Qiu, and Y. Tang, "Research on influence of metro pantograph arc on airport navigation system," *Journal of the China Railway Society*, vol. 40, no. 5, pp. 97-102, May 2018.

[11] J. Yang, "EMC experiment and protection method on control vehicle speed and distance measuring equipment of CRH2 HST," *Railway Signaling Commun. Eng*., vol. 7, no. 5, pp. 21-24, Oct. 2010.

[12] J. B. Yang, F. Zhu, J. Li, M. Sha, and D. Q. Yuan, "Electromagnetic interference measurement and analysis of high-speed electric multiple units speed sensor," *Journal of Electronic Measurement and Instrumentation*, vol. 29, no. 3, pp. 433-438, Mar. 2015.

[13] Y. Tang, F. Zhu, H. Lu, and X. Li, "Analysis and suppression of EMI for traction control unit speed sensors of CRH380BL electric multiple unit," *Applied Computational Electromagnetics Society Journal*, vol. 33, no. 5, pp. 553-560, May 2018.

[14] Y. Tang and F. Zhu, "Measurement and suppression of electromagnetic interference to speed sensor of CRH380BL electric multiple unit," *2017 International Applied Computational Electromagnetics Society Symposium*, Sept. 2017.

[15] Y. Wang, Z. Liu, X, Mu, K. Huang, and H. Wang, "An extended Habedank's equation-based EMTP model of pantograph arcing considering pantograph-catenary interactions and train speeds," *IEEE Transactions on Power Delivery*, vol. 31, no. 3, pp. 1186-1194, Jan. 2016.

[16] M. T. Cassieand D. B. Fang, "An improved arc model before current zero based on the combined Mayrand Cassiearc models," *IEEE Transactions on Power Delivery*, vol. 20, no. 1, pp. 138-142, Jan. 2005.

[17] H. Zhou, Z. Liu, Y, Cheng, and K. Huang, "Extended black-box model of pantograph arcing considering varying pantograph detachment distance," *2017 IEEE Transportation Electrification Conference and Expo, Asia-Pacific (ITEC Asia-Pacific)*, Harbin, pp. 1-6, 2017.

[18] X. Chen, B, Cao, Y. Liu, G. Gao, and G. Wu, "Dynamic model of pantograph-catenary arc of train in high speed airflow field," *High Voltage Eng*., vol. 24, no. 11, pp. 3593-3600, Nov. 2016.

[19] X. Yan, W. Chen, and Z. Li, "Simulation for self-extinction behavior of secondary arc in transmission lines," *High Voltage Eng*., vol. 38, no. 9, pp. 2150-2156, 2012.

[20] Y. Liu, G. Chang, and H. Huang, "Mayr's equation-based model for pantograph arc of high-speed railway traction system," *IEEE Transactions on Power Delivery*, vol. 25, no. 3, pp. 2025-2027, Aug. 2010.

[21] T. Zhang, "Characteristic of pantograph arcing for the high-speed train and its influence on traction drive system," *M.S. Thesis*, Dept. Electr. Eng.,

Southwest Jiaotong University, Chengdu, China, 2018.

Yutao Tang was born in Sichuan Province, China, in 1991. She received the B.S. degree in Automation from Southwest Science and Technology University, Mianyang, China, in 2013, and is currently working toward the Ph.D. degree in Electrical Engineering at Southwest Jiaotong University, Chengdu, China.

Her research interests include electromagnetic environment test and evaluation, and electromagnetic compatibility analysis and design.

Feng Zhu was born in Anhui Province, China, in 1963. He received a B.S. degree in Physics from Huaibei Normal University, Huaibei, China, in 1984, an M.S. degree in Physics from Sichuan University, Chengdu, China, in 1987, and the Ph.D. degree in Electromagnetic Theory and Microwave Techniques from Southwest Jiaotong University, Chengdu, in 1997.

He is currently a Professor in the Department of Electrical Engineering, Southwest Jiaotong University. His research interests include electromagnetic environment test and evaluation, electromagnetic compatibility, and numerical electromagnetic methods.

Yingying Chen was born in Shanxi Province, China, in 1996. She received a B.S. degree in Electrical Engineering and Automation from Taiyuan University of Science and Technology in China, in 2018. She is currently pursuing a master's degree in Electrical ngineering at Southwest Jiaotong University, Chengdu, China.

Her research interests include electromagnetic environment testing and evaluation, as well as electromagnetic compatibility analysis and design.